Science of the Total Environment 864 (2023) 161062

Contents lists available at ScienceDirect

Science of the Total Environment

journal homepage: www.elsevier.com/locate/scitotenv

Unveiling the roles of dissolved organic matters derived from different biochar in biochar/persulfate system: Mechanism and toxicity

Xuerong Zhou [a,b,c], Cui Lai [a,b,c], Eydhah Almatrafi [c], Shiyu Liu [b], Huchuan Yan [b], Shixian Qian [b], Hanxi Li [b], Lei Qin [b], Huan Yi [b], Yukui Fu [b], Ling Li [b], Mingming Zhang [b], Fuhang Xu [b], Zhuotong Zeng [a,b,c,*], Guangming Zeng [a,b,c,*]

[a] Department of Dermatology, Second Xiangya Hospital, Central South University, Changsha 410011, PR China
[b] College of Environmental Science and Engineering, Key Laboratory of Environmental Biology and Pollution Control, Hunan University, Ministry of Education, Changsha 410082, PR China
[c] Center of Research Excellence in Renewable Energy and Power Systems, Center of Excellence in Desalination Technology, Department of Mechanical Engineering, Faculty of Engineering-Rabigh, King Abdulaziz University, Jeddah 21589, Saudi Arabia

HIGHLIGHTS

- DOM on biochar exhibited pore-blocking effect in biochar/persulfate system.
- DOM on biochar suppressed the catalytic capacity of biochar.
- The elimination of DOM promoted the proportion of electron transfer process.
- The stability of biochar enhanced after removing the DOM.
- The removal of DOM reduced the toxicity of biochar/PS systems.

GRAPHICAL ABSTRACT

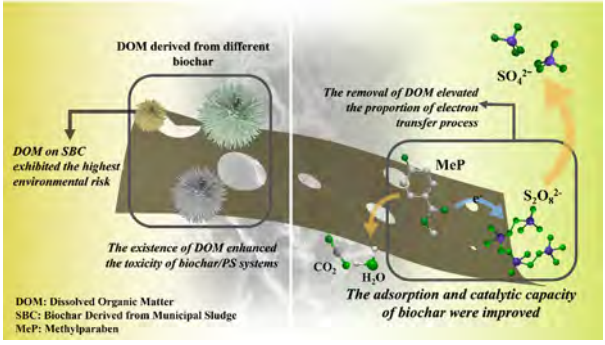

ARTICLE INFO

Editor: Daniel CW Tsang

Keywords:
Biochar
Catalysis
Dissolved organic matter
Persulfate activation
Toxicity assessment

ABSTRACT

Biochar has been frequently used as a persulfate (PS) activator due to its attractive properties, but dissolved organic matter (DOM) derived from the non-carbonized part of biochar has received less attention, not to mention its specific role and impact in biochar/PS systems. In this study, wheat straw, municipal sludge, and swine bone were selected as the representative feed stocks of biochar. Subsequently, these three types of biochar were adopted to explore the roles of DOM in biochar/PS systems. Although the composition and amount of DOM derived from different biochar were discrepant, they exhibited similar effect in biochar/PS systems. To be specific, the pore-clogging effect of DOM on biochar suppressed the adsorption capacity and catalytic performance of the three biochar. Furthermore, the removal of DOM decreased the environmental risk of these biochar/PS systems and enhanced the stability of the involved biochar. With respect to the variation in degradation mechanism, the removal of DOM increased the proportion of electron transfer pathway in unison, but the diminution in the roles of $O_2^{\cdot-}$ and $^1O_2$ was more remarkable in bone-derived-biochar/PS systems. Additionally, the toxicity test illustrated that the leakage and accumulation of DOM were toxic to *Chlorella* sp., and the DOM from sludge-derived-biochar presented the highest toxicity. Overall, this study analyzes the roles of DOM derived from different biochar in biochar/PS systems and evaluates their environmental risk, which contributes to a comprehensive understanding of the fate of DOM derived from biochar.

1. Introduction

Dissolved organic matter (DOM) universally exists in natural environment. It is recognized as an important carbon sink in the natural system (Carlson and Hansell, 2015). As is well known, DOM is valid in advanced

* Corresponding authors at: College of Environmental Science and Engineering, Hunan University, Changsha, Hunan 410082, China.
E-mail addresses: zengzhuotong@csu.edu.cn (Z. Zeng), zgming@hnu.edu.cn (G. Zeng).

http://dx.doi.org/10.1016/j.scitotenv.2022.161062
Received 15 October 2022; Received in revised form 27 November 2022; Accepted 16 December 2022
Available online 21 December 2022

oxidation processes (AOPs, such as Fenton oxidation (Wei et al., 2022), photocatalysis (Fu et al., 2022; Zhang et al., 2020), electrocatalysis (Qin et al., 2021; Wang et al., 2021), etc.) to degrade refractory pollutants.

Persulfate (PS) activation, as a trendy branch of AOPs, has gained much attention because it can overcome some blemishes of traditional Fenton system, such as strict pH limitation and sludge production (Anipsitakis and Dionysiou, 2003; Tang et al., 2017). Among numerous PS activators, biochar is considered as a promising one due to its green and low-cost properties. Current studies about the application of biochar in PS activation mainly focus on its functional structure, such as defects, oxygen-containing groups, and persistent free radicals (PFRs) (Zhou et al., 2021) However, the role of DOM derived from the uncarbonized part of biochar has been rarely investigated. In practice, DOM usually exhibits a two-sided effect in PS activation system. On the one hand, DOM can promote the decomposition of PS to generate radicals, since DOM is rich in quinones and quinones are common active sites for PS activation (Nie et al., 2022). On the other hand, DOM could hinder the degradation process by capturing the generated radicals (such as $SO_4^{\bullet-}$) (Canonica and Schönenberger, 2019). This two-sided effect of DOM makes its role in PS activation uncertain. Besides, biochar derived from different feed stocks may possess various DOM composition and amount, which may have a significant impact on PS activation. Thus, it makes sense to investigate and compare the specific role of DOM derived from different biochar in biochar/PS system. To synthesize different biochar, the common biomasses, including plant and municipal sludge (Huang et al., 2019a) were involved in this study. In addition, some unconventional biomasses, such as shrimp shell, cigarette butts, and bones, also demonstrate potential for PS activation (Yu et al., 2020; Zhou et al., 2020b). Consequently, wheat straw, municipal sludge, and swine bone were selected as the representative feed stocks to simply cover the prevailing reported biochar in this study. Moreover, it is worth noting that DOM has been reported have a certain environmental risk (He et al., 2021b), so it is also necessary to explore the negative influence of DOM on the environment.

In this study, methylparaben (MeP), a kind of pharmaceuticals and personal care product, was chosen as the target pollutant, because it is frequently detected in surface water (Soni et al., 2002; Sun et al., 2021). The biochar and biochar without DOM were involved in PS activation system to comprehend the effect of DOM on MeP degradation performance and mechanisms. The biochar and biochar without DOM were involved in PS activation system to reveal the effect of DOM on the degradation performance and mechanisms of MeP. Additionally, the characteristics (such as aromatic content, source, humification status, etc.) of DOM derived from different biochar were analyzed by fluorescence excitation-emission matrix (EEM) spectroscopy and UV–visible adsorption spectrum. At the end, their environmental risk was evaluated by *Chlorella* sp. toxicity test.

2. Materials and methods

2.1. Chemical reagent

All chemicals were applied as received, including methylparaben (MeP, 99 %), potassium peroxodisulfate (PS, 99 %), nitric acid (HNO_3, 65–68 %), hydrochloric acid (HCl, 36–38 %), hydrofluoric acid (HF, ≥ 40 %), potassium chloride (KCl, 99 %), acetonitrile (chromatographic grade), ethanol (EtOH, 99 %), tert-butyl alcohol (TBA, 99 %), *p*-benzoquinone (BQ, 99 %), sodium azide (NaN_3, 99 %), phosphate buffered saline (PBS, 10 mM) (Lin et al., 2013), potassium ferricyanide ($K_4Fe(CN)_6$, 99 %), and sodium hypochlorite (NaClO, 99 %). In addition, ultrapure water (18.25 MΩ•cm, 25 °C) was used as the solvent in this study.

2.2. Preparation of different biochar

Wheat straw, municipal sludge, and swine bone were chosen as the typical biomass of this study. All involved biomasses were heated up to the predetermined temperature at a rate of 5 °C/min and hold for 2 h (N_2 atmosphere). According to previous studies, the optimal pyrolysis temperature of different biomass was different. The use of the biochar obtained from the optimal pyrolysis temperature might be of greater practical value (Sun et al., 2021). Thus, different biomasses were carbonized in different temperature: wheat straw: 700 °C; swine bone: 900 °C; municipal sludge: 700 °C. Moreover, to avoid the influence of inorganic component and PFRs, the obtained biochar was soaked in 6 M HNO_3 for 24 h. The biochar originated from wheat straw, municipal sludge, and swine bone was marked as WBC, SBC, and BBC, respectively. The detailed process was presented in supported information (Text S1).

In order to investigate the contribution of DOM in PS activation system, DOM on biochar was wiped off with HCl and HF (Fang et al., 2017). Specifically, 2 g biochar was washed by 1 M HCl (100 mL), then it was treated with a mixture of 1 M HCl and 1 M HF (1:1 *v*/v, 100 mL). The second step repeated several times until the total organic carbon (TOC) of percolate was below the detection limit (Shimadzu TOC-L, detection limit: 4 μg/L) to make sure there was no residue DOM on biochar. Finally, the remaining salt on biochar without DOM was rinsed with ultrapure water, and then freeze-dried prior to use. The biochar that removed DOM was labeled as WBC-D, SBC-D, BBC-D.

2.3. Experimental process

Adsorption experiment was carried out to explore the adsorption characteristic: adsorption kinetics were conducted in 50 mL glass bottles, 1 g/L biochar (including BBC, SBC, WBC, BBC-D, SBC-D, and WBC-D) was mixed with 20 mg/L MeP. At each predetermined time interval (1–300 min), samples were collected and filtered by a 0.22 μm nylon filter prior to determination (all batches were launched at 298 K). The obtained data were fitted with pseudo-first-order (Eq. (1)) and pseudo-second-order (Eq. (2)) kinetic model:

$$\mathrm{In}(q_e - q_t) = \mathrm{In}q_e - k_1 t \tag{1}$$

$$\frac{t}{q_t} = \frac{1}{k_2 q_e^2} + \frac{t}{q_e} \tag{2}$$

q_e (mg/g) was the concentration of MeP at adsorption equilibrium. t (min) was the sampling time, and q_t (mg/g) was the corresponding concentration of MeP. k_1 (1/min) was the first-order rate constant, and k_2 (g/mg•min) was the second-order rate constant. Moreover, experiments were also launched to explore the adsorption isotherms (specific information was presented in supported information, Text S2).

Catalytic experimental process: To distinct the role of adsorption and degradation process, all batches would undergo a 1-h-adsorption experiment (0.1 g/L biochar was added into 20 mg/L MeP) before the catalytic process. After the adsorption process is basically completed, 1 g/L PS was applied to launch the PS activation process (all batches reacted at 298 K). Additionally, in DOM-PS test, the dosage of DOM derived from biochar (DOM—W, DOM—B, and DOM—S) was 1 g/L. All experimental conditions were referred to preliminary experiment and previous studies (Zhou et al., 2020b). Samples were collected at each predetermined interval (0, 5, 10, 15, 20, 30, 60 min), and methanol was involved to terminate radical reactions in samples. The concentration of MeP was determined by high performance liquid chromatography (HPLC) in this study. Besides, TBA, EtOH, NaN_3, and BQ were chosen as the quenching agent for •OH, $SO_4^{\bullet-}$, $^1O_2$, and $O_2^{\bullet-}$, respectively. Each degradation curve was fitted by the Langmuir-Hinshelwood model of pseudo-first-order kinetics (Eq. (3)) to make the degradation performance more intuitive.

$$\mathrm{In}\left(\frac{C_t}{C_0}\right) = -k_{obs} t \tag{3}$$

where C_t (mg/L) is the MeP concentration of samples, C_0 (mg/L) is the initial concentration (the MeP concentration after 1-h adsorption process), k_{obs} is the pseudo-first-order rate constant, and t (min) is the sampling time.

2.4. Characterization and analysis

The porous properties and specific surface area were determined by Brunauer-Emmett-Teller (BET) gas adsorption isotherm with N_2 gas (Micromeritics ASAP 2460). X-ray photoelectron spectroscopy (XPS, Thermo Scientific K-Alpha) was applied to evaluate the constituent elements of biochar. The defect level was detected by Raman spectra (Renishaw invia reflex, LabRam HR Evolution). HPLC (Agilent 1200) was equipped with C18 column (5 μm, 4.6 mm × 250 mm) to determine MeP concentration, and the mobile phase consisted of acetonitrile and water (40:60, *v*/v). Moreover, the UV detector was set as 256 nm. Electrochemical experiments were taken on a CHI760E electrochemical workstation. Thereinto, liner sweep voltammetry (LSV) experiments were performed in 10 mM PBS, while electrochemical impedance spectroscopy (EIS) experiments were conducted in a mixture of $K_4Fe(CN)_6$ and KCl (Zhou et al., 2020a). The electron spin resonance analysis (ESR, JES-FA200) was applied to confirm the existence of active species. 5,5-dimethyl-1-pyrroline N-oxide (DMPO) was the trapping agent for •OH, $SO_4^{\cdot-}$, and $O_2^{\cdot-}$, and 2,2,6,6-tetramethylpiperidine (TEMP) could capture $^1O_2$ in aqueous media.

DOM on biochar was extracted by shaker. 1 g biochar (BBC, WBC, and SBC) and 100 mL ultrapure water were added to conical flasks at room temperature. The flasks were shaken at 180 rpm for 24 h, then the suspension was filtered by 0.45 μm nylon filter. Most of the obtained liquid phase was freeze-dried to get the solid DOM, and the DOM derived from different biochar was labeled as DOM-W (DOM derived from WBC), DOM-B (DOM derived from BBC), and DOM-S (DOM derived from SBC), respectively. Furthermore, the residue leachate was collected to investigate the characteristics of DOM on different biochar. The dissolved organic carbon (DOC) of these samples was assessed by Shimadzu TOC-L. The UV–visible absorption spectrum was measured on Shimadzu UV-2700, and EEM spectroscopy was implemented on HITACHI F-7000. The emission and excitation scan were both set from 200 to 520 nm, while the stepwise was set as 5 nm. Aside from the result of EEM, the combination of UV–visible absorption and DOC could also reflect the characteristics of DOM (the specific parameters were listed in Table S2). In addition, *Chlorella* sp. was involved to assess the toxicity of biochar/PS systems and DOM derived from biochar. The specific information of toxicity experiment was presented in supported information (Text S3).

3. Results and discussion

3.1. Adsorption kinetics and isotherm

Generally, biochar possesses porous structure, which eventually leads to an excellent adsorption capacity. It was reported that the catalyst adsorption process played a vital role in PS activation systems (Liu et al., 2020a). Consequently, adsorption experiments were launched before the discussion of the catalytic performance experiments. To describe the adsorption process of different biochar, adsorption kinetics and isotherm were implemented. In the whole, the amount of MeP on biochar increased with time (Fig. S1). Moreover, the adsorption kinetics data of all involved biochar fitted pseudo-second-kinetics model better (R^2 = 0.8695–0.9926) (Table 1). It illustrated that the adsorption process was controlled by chemical sorption (Liu et al., 2015; Xu et al., 2012). Obviously, the amount of adsorbed MeP on BBC, WBC, and SBC established an uptrend after wiping off the DOM.

Table S1 and Fig. S2 presented the adsorption isotherm results of involved biochar. It showed that the adsorption process of WBC was described better by Langmuir isotherm model. Langmuir isotherm model assumed that the adsorption process belonged to monolayer adsorption on the adsorbate surface (Chen et al., 2011). However, other biochar fitted better by Freundlich isotherm model, which manifested that the multilayer adsorption prevailed in these adsorption processes (Tan et al., 2015). Furthermore, Langmuir isotherm model could be applied to estimate the maximum adsorption ability of adsorbate (Song et al., 2018), and the specific data are presented in Table S1. Compared to biochar derived from wheat straw (WBC and WBC-D) and municipal sludge (SBC and SBC-D), the biochar derived from swine bone (BBC and BBC-D) obtained a relatively high adsorption capacity (Fig. 1). The maximum adsorption ability of BBC-D could reach 172.08 mg/g. Furthermore, q_m of SBC was 25.76 mg/g, and it soared to 59.83 mg/g when DOM on SBC was removed. Similar phenomena could be observed on BBC (versus BBC-D) and WBC (versus WBC-D). Thus, it was reasonable to deduce that the elimination of DOM could promote the adsorption capacity of biochar. The elevation of adsorption capacity might owe to the blockage effect of DOM. That is, the removal of DOM created new pore structure in biochar, which is significant to the adsorption process.

Table 1
Adsorption kinetics parameters of MeP on biochar.

Samples	Pseudo-first-kinetics model			Pseudo-second-kinetics model		
	q_e (mg/g)	k_1(min^{-1})	R^2	q_e (mg/g)	k_2(g/mg•min)	R^2
BBC	82.73	0.091	0.9448	86.40	0.0020	0.9871
BBC-D	115.47	0.080	0.9751	124.59	0.0009	0.9973
WBC	1.36	0.19	0.8737	1.61	0.14	0.9174
WBC-D	2.93	0.058	0.7725	3.18	0.029	0.8695
SBC	7.44	0.10	0.9308	7.99	0.020	0.9799
SBC-D	25.03	1.25	0.9901	25.45	0.091	0.9926

Abbreviation: BBC, biochar derived from swine bone; BBC-D, biochar derived from swine bone without DOM; WBC, biochar derived from wheat straw; WBC-D, biochar derived from wheat straw without DOM; SBC, biochar derived from municipal sludge; SBC-D, biochar derived from municipal sludge without DOM.

3.2. Catalytic performance of biochar

In the past decades, biochar has been repeatedly applied in PS activation system (Zhou et al., 2021). In this study, biochar originated from different biomasses were involved to investigate the role of DOM on biochar in biochar/PS systems. According to Fig. 2a, WBC could hardly degrade MeP in PS activation system. Thus, WBC would not be involved in further discussion of degradation mechanism (including active species capture experiments and ESR spectra). In addition, the elimination of DOM could not only improve the adsorption capacity of WBC, but also could enhance its catalytic performance in PS activation system, i.e., the WBC/PS could barely degrade MeP, and WBC-D/PS system could degrade 12.18 % MeP in 60 min (k_{obs} = 0.0023 min^{-1}). Similar phenomena could also be seen in BBC/PS (versus BBC-D/PS) and SBC/PS (versus SBC-D/PS) systems. Thus, it was rational to believe that removing DOM was an effective approach to enhance the catalytic capacity of biochar. Furthermore, the

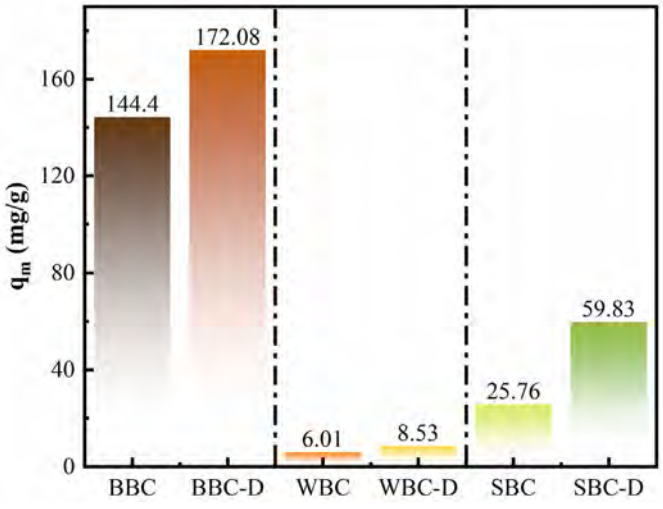

Fig. 1. The maximum adsorption ability (q_m) of involved biochar.

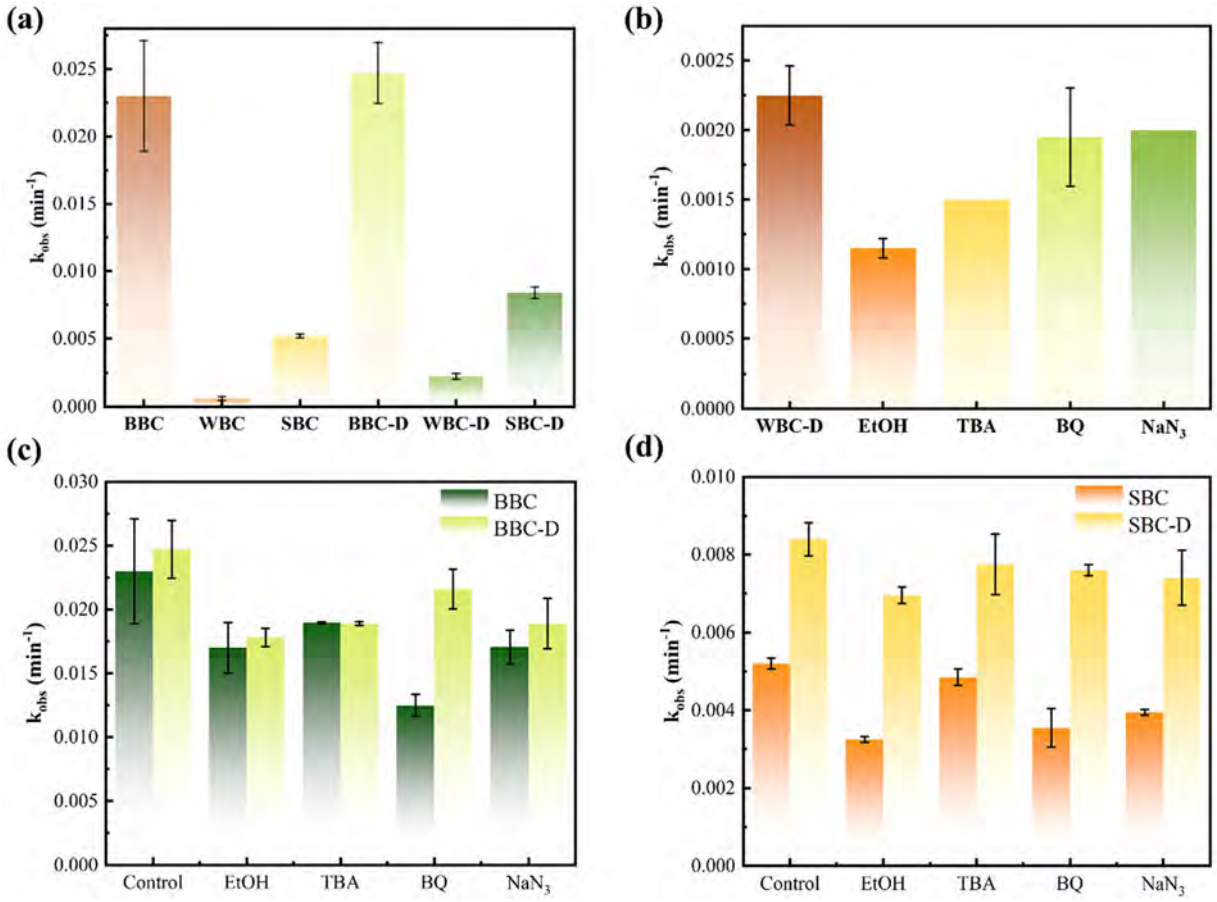

Fig. 2. (a) Catalysis performance of BBC, WBC, SBC, BBC-D, WBC-D, and SBC-D (60 min degradation process). Pseudo-first-order rate constants of active species capture experiment: (b) WBC-D, (c) BBC versus BBC-D, (d) SBC versus SBC-D. [MeP] = 20 mg/L, [PS] = 1 g/L, [biochar] = 0.1 g/L, [Temp.] = 298 K. The dosage of the quenching agents: [EtOH] = 0.75 M, [TBA] = 0.75 M, [BQ] = 1 mM, [NaN_3] = 1 mM.

catalytic capacity of biochar showed a linear positive correlation with its q_m (R^2 = 0.9905, Fig. S3a). It might support that the increase of adsorption capacity dominated the elevation of degradation rate. Besides, the DOM-PS test illustrated that DOM—W, DOM-B and DOM-S could not effectively degrade MeP in PS activation system (Fig. S3c). These phenomena collectively indicate that the enhancement in catalytic performance of biochar was mainly caused by the improvement of adsorption capacity after DOM removal, rather than DOM itself.

ESR spectra was involved to support the existence of active species. According to Fig. S4, aside from •OH and $SO_4^{\bullet-}$, $O_2^{\bullet-}$ and $^1O_2$ were also existent in all involved biochar/PS systems. Ulteriorly, active species capture experiments were taken to investigate the role of different active substances in PS activation system (Fig. 2b-d and Fig. S5b-f). TBA exhibited a relatively high reaction rate to •OH and EtOH showed high reactivity to both •OH and $SO_4^{\bullet-}$ (Li et al., 2017; Li et al., 2021). Thus, the difference in inhibitory effect of EtOH and TBA could roughly deduce the role of •OH and $SO_4^{\bullet-}$. In addition, BQ and NaN_3 exhibited uniquely high reactivity for $O_2^{\bullet-}$ and $^1O_2$, respectively. Therefore, they were selected as the quenching agent for $O_2^{\bullet-}$ and $^1O_2$. In the whole, all active species took effect in all biochar/PS systems (Fig. 2). It was in line with the results of ESR spectra. In WBC-D/PS system, the addition of EtOH declined the degradation rate from 0.0023 min^{-1} to 0.0012 min^{-1}, and TBA (0.0015 min^{-1}) showed similar inhibitory effect to EtOH. Besides, the inhibitory effect of BQ and NaN_3 was less obvious. It manifested that •OH and $SO_4^{\bullet-}$ might dominate the degradation process in WBC-D/PS system. When the BBC and SBC were denoted as the catalyst, the removal of DOM on biochar suppressed the effect of $O_2^{\bullet-}$. It might be because that DOM could induce the generation of $O_2^{\bullet-}$ in aqueous phase (Fang et al., 2013; Sun et al., 2015). To be specific, BQ abated the k_{obs} of BBC/PS system from 0.0230 min^{-1} to 0.0125 min^{-1}, and this downward trend was unpronounced in BBC-D/PS system (from 0.0247 min^{-1} to 0.0216 min^{-1}). Different from the mechanism variation in BBC/PS system (versus BBC-D/PS system), the removal of DOM weakened roles of all four active species in SBC/PS system (Fig. 2d). For example, the addition of EtOH reduced the MeP degradation rate of SBC/PS system by 36.54 % (from 0.0052 min^{-1} to 0.0033 min^{-1}), whereas that of SBC-D/PS system only declined 17.86 % (from 0.0084 min^{-1} to 0.0069 min^{-1}). Apparently, the removal of DOM derived from biochar exhibited different influence in different biochar/PS systems. It might be attributed to the difference in the amount and characteristics of DOM derived from different biochar. The specific effect of functional structures on biochar in PS activation system would be discussed in following section.

Aside from active species, electron transfer pathway has been reported as an important mechanism in PS activation system. As is well known, electron transfer pathway is an important branch of non-radical pathway in PS activation systems. It can degrade organic pollutant without producing any active species. The electron transfer pathway mainly relies on the formation of ternary system (PS, catalyst, and pollutant), and the pollutant usually acts as the electron donator (Liu et al., 2022). In this study, electrochemical experiments (LSV and EIS) were applied to evaluate electron transfer pathway. The experimental results showed that involved biochar obtained relatively high conductivity to support electron transfer pathway (except for WBC) (Fig. S6). The order of electron transfer capacity was BBC-D > BBC > WBC-D > SBC-D > SBC > WBC (Fig. 3). It was in line with the results of EIS. Based on the equivalent circuit fitting, the interface charge transfer resistance of BBC, BBC-D, WBC, WBC-D, SBC, and SBC-D were 2929, 2487, 14,370, 4342, 8275, and 5985 Ω, respectively. An obvious escalating

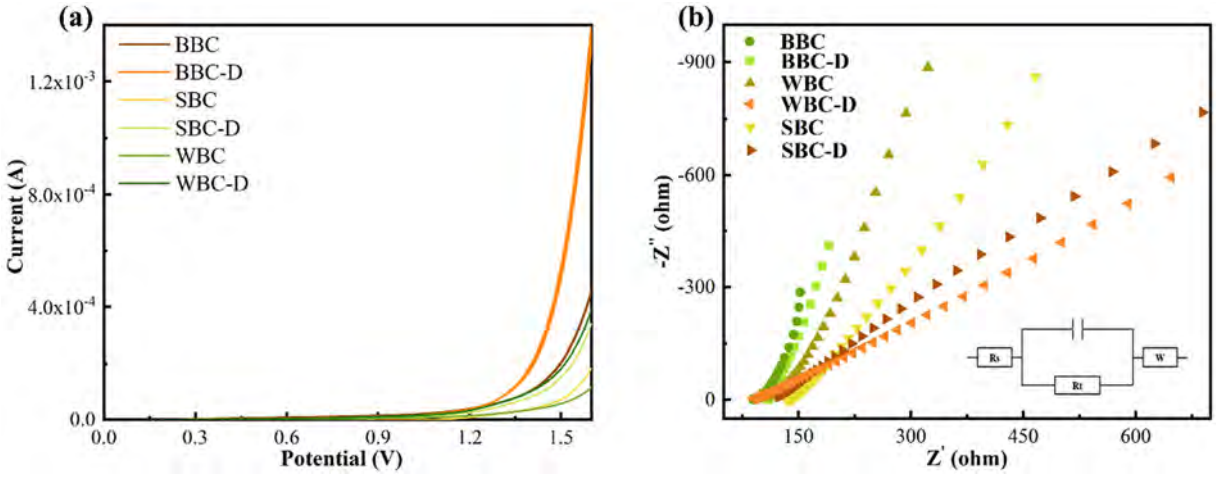

Fig. 3. (a) LSV measured with the bare GCE electrode decorated with biochar in the presence of PS and MeP, (b) EIS Nyquist plots of different biochar, frequency range from 0.01 Hz to 10^5 Hz, and the insert was the equivalent circuit diagram. [MeP] = 20 mg/L, [PS] = 1 g/L, [biochar] = 0.1 g/L, [Temp.] = 298 K.

trend of electron transfer capacity could be seen after the removal of DOM. It supported that the elimination of DOM might do favor to the electron transfer pathway, which would ultimately act on the degradation rate of MeP.

Moreover, stability test was conducted to estimate the effect of biochar derived DOM on the stability of biochar (Fig. 4). The experimental results showed that the catalytic performances of all involved biochar were decreased after 3rd run. The degradation rate decreases ratio was applied to investigate the stability of biochar. Specifically, the degradation rate of SBC exhibited a drop of 43.3 % after 3rd run, while that of SBC-D only suffered a 38.1 % reduction. Similar phenomenon could also be observed in BBC (versus BBC-D) and WBC (versus WBC-D). Therefore, it is reasonable to deduce that the removal of DOM could enhance the stability of biochar.

Subsequently, the toxicity of all involved biochar/PS systems was tested by *Chlorella* sp. According to Fig. 5, all involved biochar/PS systems significantly inhibited the growth of chlorella, and the removal of DOM derived

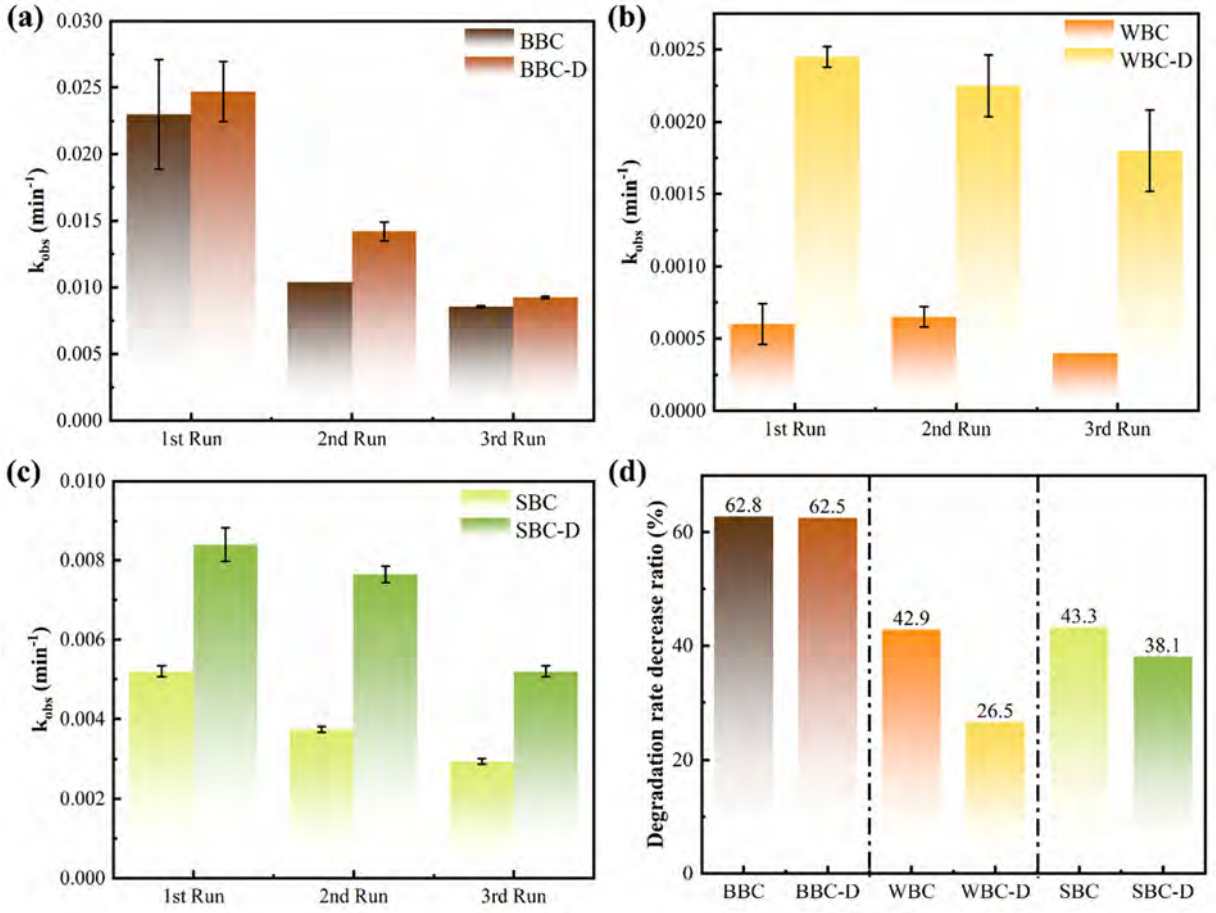

Fig. 4. Comparison of stability before and after removal of DOM: (a) BBC versus BBC-D, (b) WBC versus WBC-D, (c) SBC versus SBC-D; (d) the degradation rate decreases ratio of all involved biochar after 3rd run.

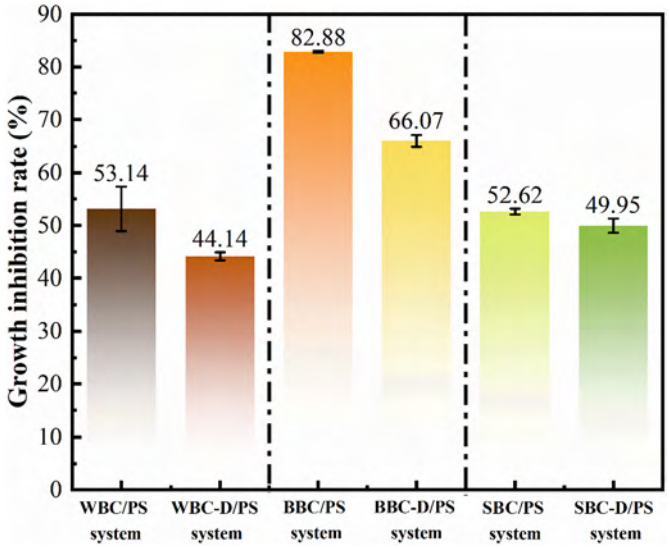

Fig. 5. The growth inhibition rate of different biochar/PS systems after a 96-h exposure.

from could suppressed the toxicity of biochar/PS system. For instance, when the DOM on BBC was removed, the Chlorella growth inhibition rate of biochar/PS system reduced from 82.88 % to 66.07 %. It might be because: 1) the removal of DOM raised proportion of less toxic electron transfer pathway (Zhou et al., 2021); 2) the DOM derived from biochar was toxic to Chlorella (He et al., 2021b). Additionally, the results of DOM toxicity test further verified that the DOM derived from different biochar all exhibited obvious toxicity (Fig. S7).

3.3. Characteristics of biochar

It is irrefutable that the catalytic performance is driven by the functional structures on biochar. Pore structure, defects, and oxygen-containing groups are denoted as the active sites in biochar/PS systems (Zhou et al., 2021). Given these, the characteristics of biochar were taken into consideration to probe the mechanism of biochar/PS system.

Pore volume and specific surface area of these biochar samples were measured by N_2 adsorption and desorption analysis (Table 2). The results manifested that the specific surface area and pore volume of BBC (versus BBC-D) soared from 1024.34 m^2/g and 0.8118 cm^3/g to 1201.63 m^2/g and 0.9322 cm^3/g. Similar phenomena could be observed in WBC (versus WBC-D) and SBC (versus SBC-D). Since mineral was removed in pretreatment, DOM removal became the main cause of the improvement of specific surface area. Furthermore, the amplification of surface area might be also responsible for the promotion of electron transfer pathway in DOM-removed biochar/PS system. It was reported that the adsorption capacity of catalyst was closely related to the oxidation ability of electron transfer pathway (Ren et al., 2020). Furthermore, the extremely low specific surface area of WBC might associate with its deficiency in adsorption isotherm (mentioned in Section 3.1). Notably, the specific surface area of biochar was positively correlated with their q_m (Fig. S3b). It revealed the close relationship between the pore structure and adsorption capacity of biochar. Noteworthy, the other functional structures on biochar also played indispensable roles in PS activation system (Zhou et al., 2020b).

Table 2
Pore structure and specific surface area of biochar.

Samples	Specific surface area (m^2/g)	Pore volume (cm^3/g)	Elemental composition (%)	
			C	O
BBC	1024.34	0.81	89.63	10.37
WBC	15.52	0.012	86.41	13.59
SBC	244.30	0.30	68.30	31.70
BBC-D	1201.63	0.93	90.92	9.08
WBC-D	143.19	0.13	91.22	8.78
SBC-D	387.02	0.51	85.29	14.71

Abbreviation: BBC, biochar derived from swine bone; BBC-D, biochar derived from swine bone without DOM; WBC, biochar derived from wheat straw; WBC-D, biochar derived from wheat straw without DOM; SBC, biochar derived from municipal sludge; SBC-D, biochar derived from municipal sludge without DOM.

Raman spectra was applied to probe into the defective degree of involved biochar. As shown in Fig. 6, the Raman spectra was deconvoluted into six characteristic peaks. Specifically, S band (1290 cm^{-1}) indicated the change of sp^2 to sp^3 in the carbon lattice; D band (1350 cm^{-1}) ascribed to the defect structure; V_1 band (1520 cm^{-1}) and V_2 band (1545 cm^{-1}) assigned to amorphous carbon and the semicircle ring breathing, respectively; G_1 band (1590 cm^{-1}) represented to the aromatic structure with 3–5 rings; G_2 band (1620 cm^{-1}) indicated the highly ordered aromatics (Wan et al., 2019; Yang et al., 2018). A_D/A_G was applied to index the graphitization degree of carbonaceous materials (Wan et al., 2021). The A_D/A_G value of BBC was 3.13, and it decreased to 2.55 after removing the DOM. Similar phenomenon was also observed for WBC and SBC. Thus, the removal of DOM increased the graphitization degree and declined the defective degree of biochar. Furthermore, the defect structure was elaborately indexed by A_D/A_V. The relatively high A_D/A_V value indicated a high proportion of vacancies in carbon lattice, and the low A_D/A_V assigned to a high density of boundary edges (the threshold was 3.5) (Eckmann et al., 2012). The A_D/A_V value of all involved biochar were lower than 3.5, it illustrated that the edge defects were the dominant defects. In general, the edge defects on biochar could act as the active sites for $^1O_2$ and $O_2^{\cdot-}$ in PS activation systems (Cheng et al., 2019; Ouyang et al., 2019). However, the catalytic performance supported that the decrease of defective level did not lead to a decrement in the degradation rate of biochar/PS systems. Furthermore, the relatively low defective degree resulting from the DOM removal did not lead to a relatively large proportion of $^1O_2$ and $O_2^{\cdot-}$ in biochar/PS systems (Fig. 2). It hinted that the defect introduced by DOM was not the dominant active site in all involved biochar/PS system.

The element component of biochar would also influence its behavior in the environment (Chen et al., 2008; Xiao et al., 2016). The variation of element components is roughly exhibited in Table 2. The uncarbonized partition of biochar was the primary source of DOM on biochar, which would ultimately contribute to the oxygen content. The relatively low oxygen content on BBC-D, WBC-D, and SBC-D might associate with the removal of DOM. Whereas the oxygen content in BBC only decreased 1 % after the elimination of DOM, it might owe to the higher annealing temperature of BBC (Zhu et al., 2018).

Except for the oxygen content, the removal of DOM would also alter the proportion of different oxygen-containing groups. To further present the change in oxygen-containing groups before and after DOM removal, O 1 s high resolution spectra were involved to investigate the variation of oxygen-containing groups on biochar. As shown in Fig. 7, the peak appeared around 533 eV could be ascribed to oxygen, and it could be divided into two peaks (López et al., 1991). Specifically, peaks around 531.5 eV and 533.3 eV represented the vibration of C—O and C═O, respectively. With respect to SBC and SBC-D, the elimination of DOM elevated the proportion of C—O from 9.37 % to 50.36 %. It might owe to the removal of quinone moieties, for quinone moieties were appointed as an important component in DOM (Liu et al., 2020b). Similar phenomenon could be seen in WBC and WBC-D. Conversely, comparing to BBC, the C—O proportion of BBC-D was lower. The difference in the constituent of biomass might be account for this distinction. Specifically, the pyrolysis of cellulose (the main ingredient of wheat straw) would induce the production of ketones (such as furanones and cyclopentanones) (Chen et al., 2019b). In addition, it was reported that the *co*-pyrolysis of polysaccharide and amino acids (composition of municipal sludge) would facilitate the generation of aldehydes (such as 5-methylfurfural) (Chen et al., 2019a). Different from wheat straw and municipal sludge, the organic component of swine bone was principally

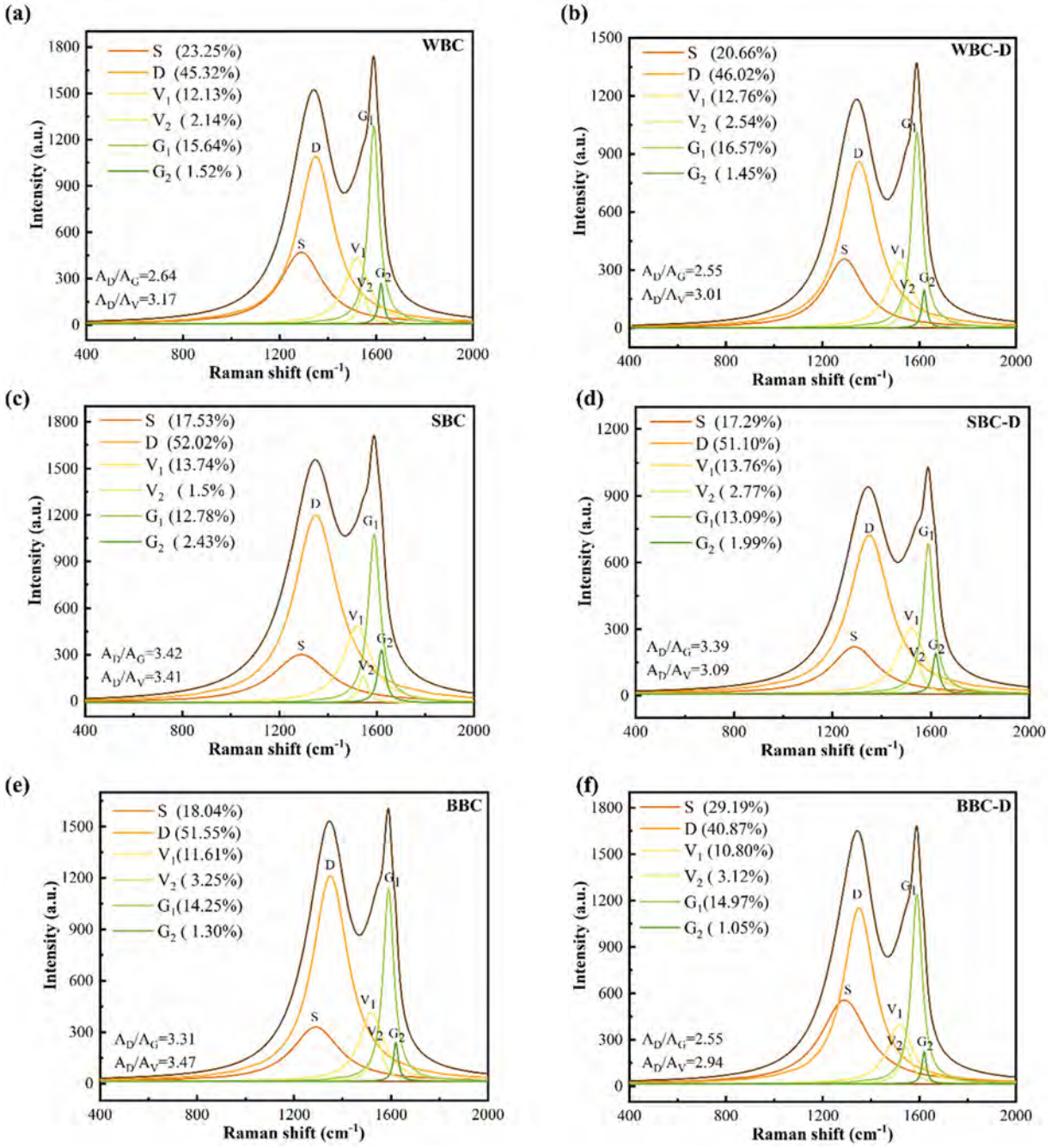

Fig. 6. Deconvoluted Raman spectra of (a) WBC, (b) WBC-D, (c) SBC, (d) SBC-D, (e) BBC, and (f) BBC-D.

constituted by proline, glycine, hydroxyproline, and alanine amino acids (Huang et al., 2019b). These amino acids prefer to produce gas (such as CO_2) rather than C═O.

The DOM removal process (HF and HCl treatment) was deemed to have effect on oxygen-containing groups on biochar. Generally, acid treatment (including HF and HCl) would enhance the proportion of acid groups (such as -COOH and -OH) on biochar surface which could act as the active sites for radical pathway (•OH and $SO_4^{\bullet-}$) in PS activation systems (Zhou et al., 2021). However, the treatment of HF and HCl did not significantly increase the proportion of acid groups (Fig. 7) on biochar and the proportion of radical pathway in PS activation system (Fig. 2). Thus, the effect of HF-HCl treatment on oxygen-containing groups was deemed to be negligible.

As for catalytic performance, generally, C═O (including carboxyl, ketones, aldehydes) on carbonaceous materials was reported as the active site for electron transfer pathway (Zhou et al., 2020b). According to Fig. 7, the increase of C═O proportion on BBC (versus BBC-D) did promote the electron transfer pathway. However, although the C═O content of SBC declined after DOM removal (versus SBC-D), it was not suppressed the electron transfer pathway. Similarly, the decrease of C═O proportion did not weaken the electron transfer pathway of WBC/PS system. As mentioned above, specific surface area could also influence the electron transfer pathway. It might dominate the variation of electron transfer pathway in WBC/PS and SBC/PS systems. Consequently, even if the amount of C═O was decreased, the proportion of electron transfer pathway did not sink. Overall, although C═O can be denoted as the active site for electron transfer pathway, the effect of C═O was not reflected in WBC/PS and SBC/PS systems. In addition, the increased C═O and specific surface area together contributed the ascent of electron transfer pathway in BBC/PS system (Scheme 1).

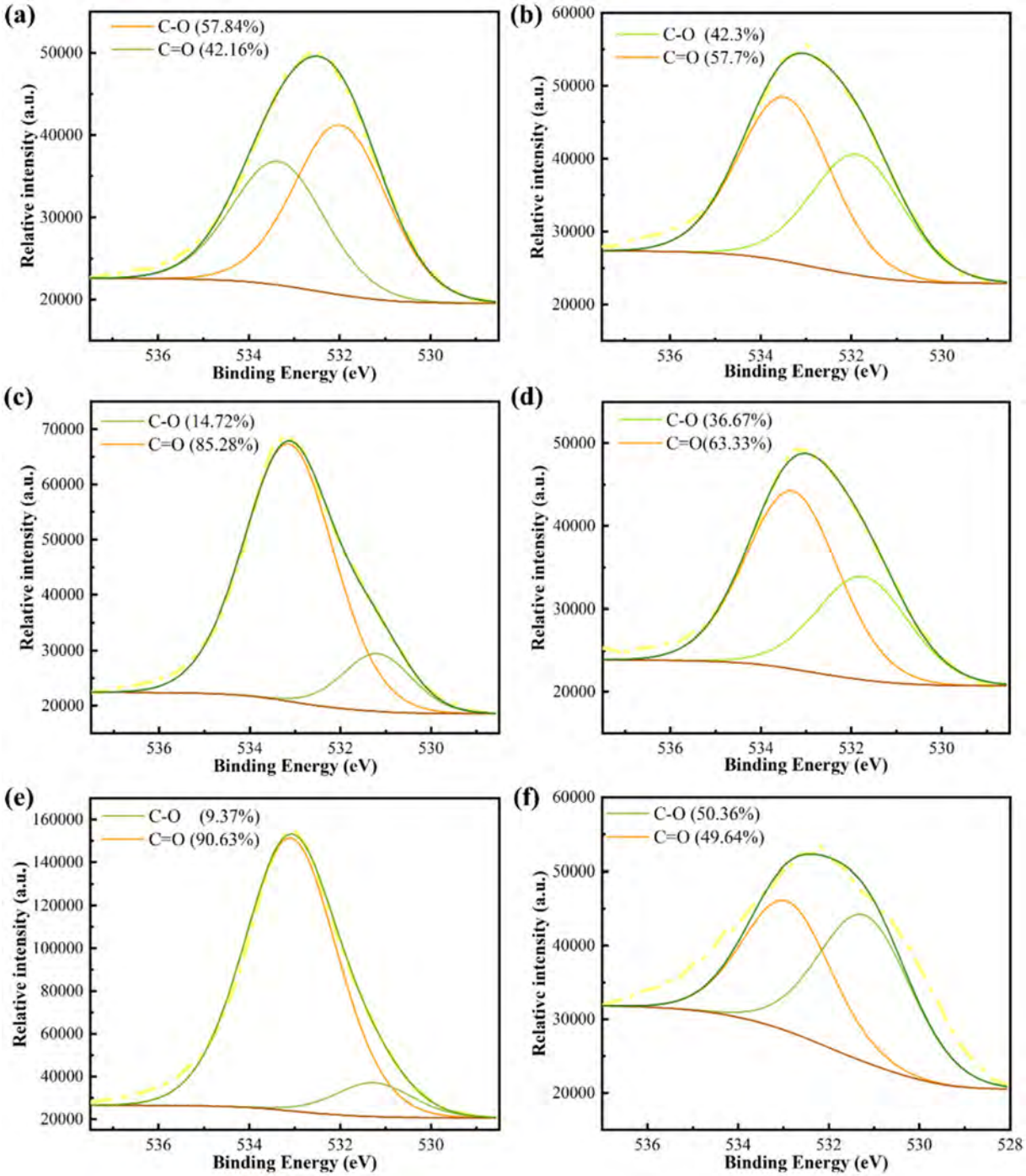

Fig. 7. O 1 s spectra of (a) BBC, (b) BBC-D, (c) WBC, (d) WBC-D, (e) SBC, and (f) SBC-D.

3.4. Properties of dissolved organic matters derived from different biochar

As discussed above, apparently, the elimination of DOM enhanced both adsorption capacity and catalytic performance of biochar. Furthermore, the removal of DOM reduced the toxicity of biochar/PS system and enhanced the stability of biochar. However, there were subtle differences in the effects of DOM derived from different biochar, which might associate with the different properties of DOM.

DOC was applied to evaluate the quantity of organic matter on different biochar. As shown in Fig. 8, DOC of BBC leachate was 7.618 mg/L, and that of WBC and SBC leachates was 106.147 and 38.139 mg/L, respectively. The conspicuous difference in DOC might associate with the difference in annealing temperature and biochar source. The relatively high annealing temperature of BBC could carbonize more organic components in feed stock. As a result, the amount of DOM derived from BBC was the least. Combined with the result of catalytic performance, it is reasonable to deduce that the more DOM leached from biochar would induce a higher catalytic performance of biochar.

As is well-known, the EEM spectra (Fig. S8) could give more information about the DOM (such as the aromatic content, source, and humification status, the information of different parameters was listed in Table S2) (Inamdar et al., 2012). Table 3 summarized the properties of DOM derived from different biochar. It has been reported that $SUVA_{254}$ was correlated with aromatic carbon and macromolecules organic matters (Zhang et al., 2014). The

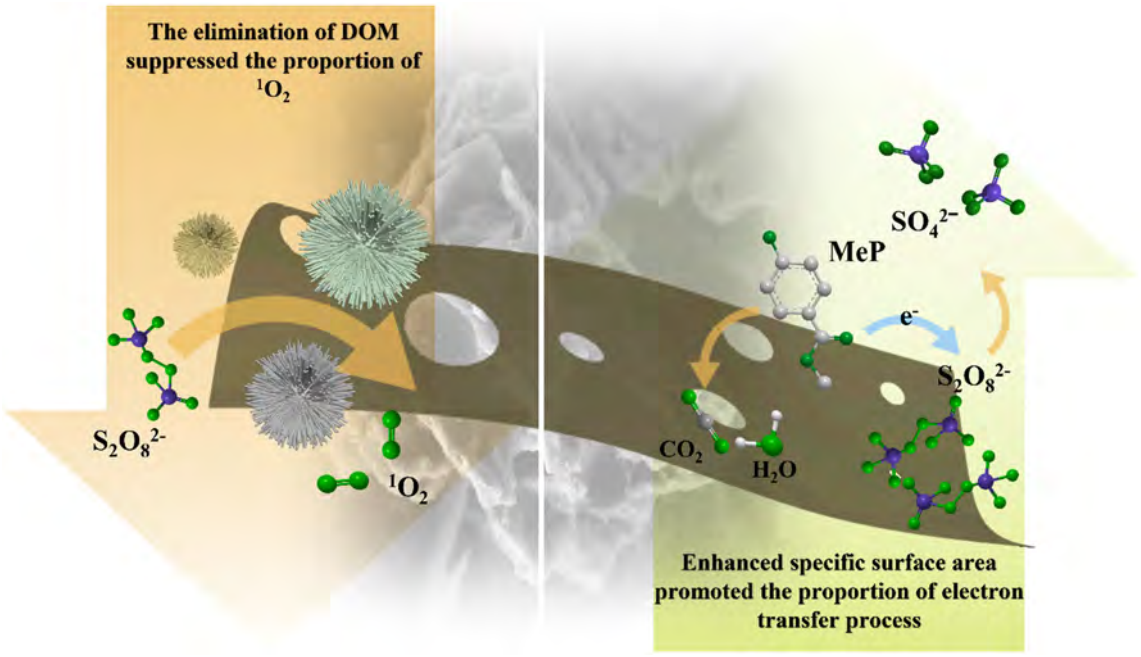

Scheme 1. The mainly roles of DOM derived from biochar in PS activation system.

$SUVA_{254}$ of BBC was eminently higher than WBC and SBC. As mentioned above, the higher aromatization of BBC-derived DOM might owe to the higher annealing temperature of BBC. Analogously, the considerably high $SUVA_{260}$ of DOM derived from BBC indexed a higher proportion of hydrophobic components, which also indicated a relatively high degree of aromatization. Furthermore, FI could index the source of DOM, while the value of FI lower than 1.4 represents the predominance of terrestrial fulvic acids (Zhang et al., 2010). The DOM derived from BBC, WBC, and SBC all had apparent characteristics of terrestrial origin. To evaluate the humification status and maturity of DOM, HIX was involved. It has been reported that HIX ranged from 0 to 1, and the high HIX value signified the high humification and stability of DOM (Ohno, 2002). Compared with the DOM originated from natural environment (in the range of 0.5–0.9), the HIX values of DOM derived from BBC, WBC, and SBC were critically low (Huguet et al., 2009; Yang et al., 2015). It hinted that the DOM derived from biochar was instable in the environment. As is well-known, the DOM leaching from biochar might be toxic to organisms (He et al., 2021a; Smith et al., 2013). Consequently, it is essential to evaluate the environmental risk of DOM derived from biochar.

In this study, the growth inhibition rate of *Chlorella* sp. was involved to roughly investigate the environmental risk of DOM derived from different biochar (Fig. S7). The growth inhibition rate of DOM derived from BBC, WBC, and SBC was 45.76 %, 31.59 %, and 58.73 %, respectively. Unexpectedly, DOM derived from SBC possessed the highest environmental risk. Although the amount of DOM on WBC was the highest, its inhibitory effect on algae growth was the weakest. It supported that WBC might be an eco-friendly alternate. As a result, DOM derived from biochar all possessed environmental risk, and it would change with the variation of feed stock. To promote the green application of biochar, it is necessary to assign the DOM toxicity as a basis of biochar selection.

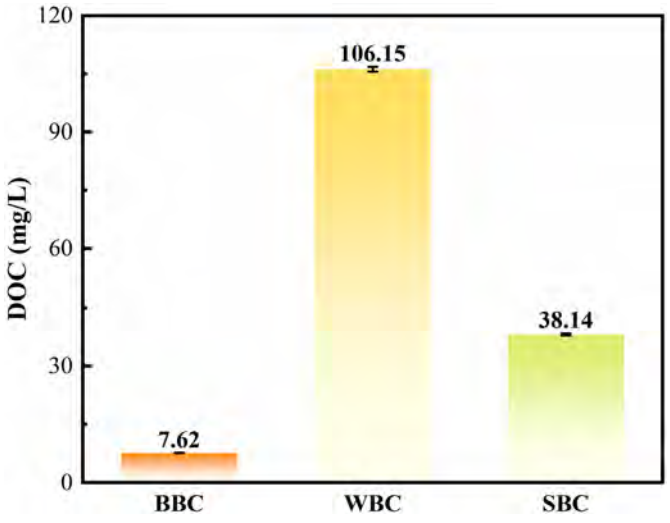

Fig. 8. The DOC of DOM derived from different biochar.

4. Conclusions

In this study, the role of DOM derived from different biochar in PS activation system was comprehensively evaluated. Overall, among the effect brought about by DOM, the pore-blocking effect was the most obvious in PS activation systems. And the existence of DOM derived from biochar suppressed the adsorption capacity and catalytic performance of biochar. Furthermore, the elimination of DOM on biochar could commonly reduce the toxicity of biochar/PS system. It might be ascribed to the removal of toxic DOM and the variation in degradation mechanism. With respect to the specific mechanism, the removal of DOM increased the proportion of electron transfer pathway, which was owe to the lifting of biochar specific surface area. The properties of DOM on biochar itself were also studied.

Table 3
Spectroscopic properties of DOM derived from different biochar.

Samples	$SUVA_{254}$ (L/mg•m)	$SUVA_{260}$ (L/mg•m)	Fluorescence index (FI)	Humification index (HIX)
BBC	9.957	5.960	1.305	0.166
WBC	0.533	0.478	1.207	0.193
SBC	1.128	1.484	1.086	0.187

Abbreviation: BBC, biochar derived from swine bone; WBC, biochar derived from wheat straw; SBC, biochar derived from municipal sludge.

None of the involved DOM could effectively activate PS. Although the composition and quantity were different, the DOM derived from different biochar displayed terrestrial origin and relatively low humification degree. Moreover, in the toxicity assessment, the DOM derived from SBC was the most toxic. To sum up, DOM on biochar conspicuously influenced the environmental risk and degradation performance of biochar/PS system. Consequently, it is necessary to evaluate the integrative role of DOM derived from biochar before downstream application.

CRediT authorship contribution statement

Xuerong Zhou: Writing, methodology, investigation, analysis, original draft

Cui Lai: Writing, methodology, investigation, review and editing

Eydhah Almatrafi: Methodology, review and editing

Shiyu Liu: Methodology, review and editing

Huchuan Yan: Investigation, review and editing

Shixian Qian: Investigation, review and editing

Hanxi Li: Investigation, review and editing

Lei Qin: Investigation, review and editing

Huan Yi: Investigation, review and editing

Yukui Fu: Methodology, review and editing

Ling Li: Methodology, review and editing

Mingming Zhang: Methodology, review and editing

Fuhang Xu: Methodology, investigation, analysis

Zhuotong Zeng: Writing, methodology, investigation, review and editing

Guangming Zeng: Writing, methodology, investigation, review and editing

Data availability

Data will be made available on request.

Declaration of competing interest

The authors declare that they have no known competing financial interests or personal relationships that could have appeared to influence the work reported in this paper.

Acknowledgements

This study was financially supported by the Program for the National Natural Science Foundation of China (82003363, U20A20323, 52170161, 51879101), the Program for Changjiang Scholars and Innovative Research Team in University (IRT-13R17), and Hunan Provincial Science and Technology Plan Project (2018SK20410), Hunan Provincial Natural Science Foundation (S2021JJQNJJ2330, S2020JJ3009), and the Changsha Municipal Natural Science Foundation (kq2007059).

Appendix A. Supplementary data

Supplementary data to this article can be found online at https://doi.org/10.1016/j.scitotenv.2022.161062.

References

Anipsitakis, G.P., Dionysiou, D.D., 2003. Degradation of organic contaminants in water with sulfate radicals generated by the conjunction of peroxymonosulfate with cobalt. Environ. Sci. Technol. 37, 4790–4797.

Canonica, S., Schönenberger, U., 2019. Inhibitory effect of dissolved organic matter on the transformation of selected anilines and sulfonamide antibiotics induced by the sulfate radical. Environ. Sci. Technol. 53, 11783–11791.

Carlson, C.A., Hansell, D.A., 2015. Chapter 3 - DOM sources, sinks, reactivity, and budgets. In: Hansell, D.A., Carlson, C.A. (Eds.), Biogeochemistry of Marine Dissolved Organic Matter, (Second Edition) Academic Press, Boston, pp. 65–126.

Chen, B., Zhou, D., Zhu, L., 2008. Transitional adsorption and partition of nonpolar and polar aromatic contaminants by biochars of pine needles with different pyrolytic temperatures. Environ. Sci. Technol. 42, 5137–5143.

Chen, X., Chen, G., Chen, L., Chen, Y., Lehmann, J., McBride, M.B., et al., 2011. Adsorption of copper and zinc by biochars produced from pyrolysis of hardwood and corn straw in aqueous solution. Bioresour. Technol. 102, 8877–8884.

Chen, H., Xie, Y., Chen, W., Xia, M., Li, K., Chen, Z., et al., 2019a. Investigation on co-pyrolysis of lignocellulosic biomass and amino acids using TG-FTIR and py-GC/MS. Energy Convers. Manag. 196, 320–329.

Chen, L., Liao, Y., Guo, Z., Cao, Y., Ma, X., 2019b. Products distribution and generation pathway of cellulose pyrolysis. J. Clean. Prod. 232, 1309–1320.

Cheng, X., Guo, H., Zhang, Y., Korshin, G.V., Yang, B., 2019. Insights into the mechanism of nonradical reactions of persulfate activated by carbon nanotubes: activation performance and structure-function relationship. Water Res. 157, 406–414.

Eckmann, A., Felten, A., Mishchenko, A., Britnell, L., Krupke, R., Novoselov, K.S., et al., 2012. Probing the nature of defects in graphene by Raman spectroscopy. Nano Lett. 12, 3925–3930.

Fang, G., Gao, J., Dionysiou, D.D., Liu, C., Zhou, D., 2013. Activation of persulfate by quinones: free radical reactions and implication for the degradation of PCBs. Environ. Sci. Technol. 47, 4605–4611.

Fang, G., Liu, C., Wang, Y., Dionysiou, D.D., Zhou, D., 2017. Photogeneration of reactive oxygen species from biochar suspension for diethyl phthalate degradation. Appl. Catal. B Environ. 214, 34–45.

Fu, Y., Yin, Z., Qin, L., Huang, D., Yi, H., Liu, X., et al., 2022. Recent progress of noble metals with tailored features in catalytic oxidation for organic pollutants degradation. J. Hazard. Mater. 422, 126950.

He, M., Wan, Z., Tsang, D.C., Sun, Y., Khan, E., Hou, D., et al., 2021a. Performance indicators for a holistic evaluation of catalyst-based degradation—a case study of selected pharmaceuticals and personal care products (PPCPs). J. Hazard. Mater. 402, 123460.

He, M., Xiong, X., Wang, L., Hou, D., Bolan, N.S., Ok, Y.S., et al., 2021b. A critical review on performance indicators for evaluating soil biota and soil health of biochar-amended soils. J. Hazard. Mater. 414, 125378.

Huang, M., Li, Z., Luo, N., Yang, R., Wen, J., Huang, B., et al., 2019a. Application potential of biochar in environment: insight from degradation of biochar-derived DOM and complexation of DOM with heavy metals. Sci. Total Environ. 646, 220–228.

Huang, W., Restrepo, D., Jung, J.Y., Su, F.Y., Liu, Z., Ritchie, R.O., et al., 2019b. Multiscale toughening mechanisms in biological materials and bioinspired designs. Adv. Mater. 31, e1901561.

Huguet, A., Vacher, L., Relexans, S., Saubusse, S., Froidefond, J.M., Parlanti, E., 2009. Properties of fluorescent dissolved organic matter in the gironde estuary. Org. Geochem. 40, 706–719.

Inamdar, S., Finger, N., Singh, S., Mitchell, M., Levia, D., Bais, H., et al., 2012. Dissolved organic matter (DOM) concentration and quality in a forested mid-Atlantic watershed, USA. Biogeochemistry 108, 55–76.

Li, D., Duan, X., Sun, H., Kang, J., Zhang, H., Tade, M.O., et al., 2017. Facile synthesis of nitrogen-doped graphene via low-temperature pyrolysis: the effects of precursors and annealing ambience on metal-free catalytic oxidation. Carbon 115, 649–658.

Li, L., Liu, S., Cheng, M., Lai, C., Zeng, G., Qin, L., et al., 2021. Improving the Fenton-like catalytic performance of MnOx-Fe3O4/biochar using reducing agents: a comparative study. J. Hazard. Mater. 406, 124333.

Lin, X., Tan, L., Zhang, Q., Yang, K., Hu, Z., Qiu, J., et al., 2013. The in vitro degradation process and biocompatibility of a ZK60 magnesium alloy with a forsterite-containing micro-arc oxidation coating. Acta Biomater. 9, 8631–8642.

Liu, B., Peng, X., Chen, W., Li, Y., Meng, X., Wang, D., et al., 2015. Adsorptive removal of patulin from aqueous solution using thiourea modified chitosan resin. Int. J. Biol. Macromol. 80, 520–528.

Liu, S., Lai, C., Li, B., Zhang, C., Zhang, M., Huang, D., et al., 2020a. Role of radical and nonradical pathway in activating persulfate for degradation of p-nitrophenol by sulfur-doped ordered mesoporous carbon. Chem. Eng. J. 384.

Liu, X., Liu, R., Zhu, B., Ruan, T., Jiang, G., 2020b. Characterization of carbonyl disinfection by-products during ozonation, chlorination, and chloramination of dissolved organic matters. Environ Sci Technol 54, 2218–2227.

Liu, S., Lai, C., Zhou, X., Zhang, C., Chen, L., Yan, H., et al., 2022. Peroxydisulfate activation by sulfur-doped ordered mesoporous carbon: insight into the intrinsic relationship between defects and (1)O2 generation. Water Res. 221, 118797.

López, G.P., Castner, D.G., Ratner, B.D., 1991. XPS O 1s binding energies for polymers containing hydroxyl, ether, ketone and ester groups. Surf. Interface Anal. 17, 267–272.

Nie, J., Zou, J., Yan, S., Song, W., 2022. Photosensitized transformation of peroxymonosulfate in dissolved organic matter solutions under simulated solar irradiation. Environ. Sci. Technol. 56, 1963–1972.

Ohno, T., 2002. Fluorescence inner-filtering correction for determining the humification index of dissolved organic matter. Environmental Science & Technology 36, 742–746.

Ouyang, D., Chen, Y., Yan, J., Qian, L., Han, L., Chen, M., 2019. Activation mechanism of peroxymonosulfate by biochar for catalytic degradation of 1,4-dioxane: important role of biochar defect structures. Chem. Eng. J. 370, 614–624.

Qin, L., Wang, Z., Fu, Y., Lai, C., Liu, X., Li, B., et al., 2021. Gold nanoparticles-modified MnFe2O4 with synergistic catalysis for photo-Fenton degradation of tetracycline under neutral pH. J. Hazard. Mater. 414, 125448.

Ren, W., Xiong, L., Nie, G., Zhang, H., Duan, X., Wang, S., 2020. Insights into the electron-transfer regime of peroxydisulfate activation on carbon nanotubes: the role of oxygen functional groups. Environ Sci Technol 54, 1267–1275.

Smith, C.R., Buzan, E.M., Lee, J.W., 2013. Potential impact of biochar water-extractable substances on environmental sustainability. ACS Sustain. Chem. Eng. 1, 118–126.

Song, B., Xu, P., Zeng, G., Gong, J., Wang, X., Yan, J., et al., 2018. Modeling the transport of sodium dodecyl benzene sulfonate in riverine sediment in the presence of multi-walled carbon nanotubes. Water Res. 129, 20–28.

Soni, M.G., Taylor, S.L., Greenberg, N.A., Burdock, G.A., 2002. Evaluation of the health aspects of methyl paraben: a review of the published literature. Food Chem. Toxicol. 40, 1335–1373.
Sun, L., Qian, J., Blough, N.V., Mopper, K., 2015. Insights into the photoproduction sites of hydroxyl radicals by dissolved organic matter in natural waters. Environ. Sci. Technol. Lett. 2, 352–356.
Sun, Y., Xiong, X., He, M., Xu, Z., Hou, D., Zhang, W., et al., 2021. Roles of biochar-derived dissolved organic matter in soil amendment and environmental remediation: a critical review. Chem. Eng. J. 424, 130387.
Tan, X., Liu, Y., Zeng, G., Wang, X., Hu, X., Gu, Y., et al., 2015. Application of biochar for the removal of pollutants from aqueous solutions. Chemosphere 125, 70–85.
Tang, L., Feng, H., Tang, J., Zeng, G., Deng, Y., Wang, J., et al., 2017. Treatment of arsenic in acid wastewater and river sediment by Fe@Fe2O3 nanobunches: the effect of environmental conditions and reaction mechanism. Water Res. 117, 175–186.
Wan, Z., Sun, Y., Tsang, D.C., Iris, K., Fan, J., Clark, J.H., et al., 2019. A sustainable biochar catalyst synergized with copper heteroatoms and CO2 for singlet oxygenation and electron transfer routes. Green Chem. 21, 4800–4814.
Wan, Z., Xu, Z., Sun, Y., He, M., Hou, D., Cao, X., et al., 2021. Critical impact of nitrogen vacancies in nonradical carbocatalysis on nitrogen-doped graphitic biochar. Environ. Sci. Technol. 55, 7004–7014.
Wang, D., He, N., Xiao, L., Dong, F., Chen, W., Zhou, Y., et al., 2021. Coupling electrocatalytic nitric oxide oxidation over carbon cloth with hydrogen evolution reaction for nitrate synthesis. Angew. Chem. 133, 24810–24816.
Wei, X., Yi, H., Lai, C., Huo, X., Ma, D., Du, C., 2022. Synergistic effect of flower-like MnFe2O4/MoS2 on photo-Fenton oxidation remediation of tetracycline polluted water. J. Colloid Interface Sci. 608, 942–953.
Xiao, X., Chen, Z., Chen, B., 2016. H/C atomic ratio as a smart linkage between pyrolytic temperatures, aromatic clusters and sorption properties of biochars derived from diverse precursory materials. Sci. Rep. 6, 22644.
Xu, P., Zeng, G.M., Huang, D.L., Feng, C.L., Hu, S., Zhao, M.H., et al., 2012. Use of iron oxide nanomaterials in wastewater treatment: a review. Sci. Total Environ. 424, 1–10.
Yang, L., Chang, S.-W., Shin, H.-S., Hur, J., 2015. Tracking the evolution of stream DOM source during storm events using end member mixing analysis based on DOM quality. J. Hydrol. 523, 333–341.
Yang, X., Igalavithana, A.D., Oh, S.-E., Nam, H., Zhang, M., Wang, C.-H., et al., 2018. Characterization of bioenergy biochar and its utilization for metal/metalloid immobilization in contaminated soil. Sci. Total Environ. 640, 704–713.
Yu, J.F., Tang, L., Pang, Y., Zeng, G.M., Feng, H.P., Zou, J.J., et al., 2020. Hierarchical porous biochar from shrimp shell for persulfate activation: a two-electron transfer path and key impact factors. Appl. Catal. B Environ. 260.
Zhang, Y., Zhang, E., Yin, Y., Van Dijk, M.A., Feng, L., Shi, Z., et al., 2010. Characteristics and sources of chromophoric dissolved organic matter in lakes of the yungui plateau, China, differing in trophic state and altitude. Limnol. Oceanogr. 55, 2645–2659.
Zhang, J., Lü, F., Luo, C., Shao, L., He, P., 2014. Humification characterization of biochar and its potential as a composting amendment. J. Environ. Sci. 26, 390–397.
Zhang, M., Lai, C., Li, B., Xu, F., Huang, D., Liu, S., et al., 2020. Unravelling the role of dual quantum dots cocatalyst in 0D/2D heterojunction photocatalyst for promoting photocatalytic organic pollutant degradation. Chem. Eng. J. 396, 125343.
Zhou, X., Zeng, Z., Zeng, G., Lai, C., Xiao, R., Liu, S., et al., 2020a. Persulfate activation by swine bone char-derived hierarchical porous carbon: multiple mechanism system for organic pollutant degradation in aqueous media. Chem. Eng. J. 383.
Zhou, X., Zeng, Z., Zeng, G., Lai, C., Xiao, R., Liu, S., et al., 2020b. Insight into the mechanism of persulfate activated by bone char: unraveling the role of functional structure of biochar. Chem. Eng. J. 401, 126127.
Zhou, X., Zhu, Y., Niu, Q., Zeng, G., Lai, C., Liu, S., et al., 2021. New notion of biochar: a review on the mechanism of biochar applications in advannced oxidation processes. Chem. Eng. J. 416.
Zhu, S., Huang, X., Ma, F., Wang, L., Duan, X., Wang, S., 2018. Catalytic removal of aqueous contaminants on N-doped graphitic biochars: inherent roles of adsorption and nonradical mechanisms. Environ Sci Technol 52, 8649–8658.